INSTITUTE OF PHYSICS PUBLISHING PLASMA SOURCES SCIENCE AND TECHNOLOGY

Plasma Sources Sci. Technol. **10** (2001) 417–422 PII: S0963-0252(01)21957-4

Helicon plasma generation at very high radio frequency

G S Eom[1], I D Bae[1,3], G Cho[1], Y S Hwang[2] and W Choe[1,4]

[1] Tokamak and Applied Plasma Laboratory, Korea Advanced Institute of Science and Technology, 373-1 Kusong-dong, Yusong-gu, Taejon 305-701, Korea
[2] Seoul National University, San 56-1 Shilim-dong, Kwanak-gu, Seoul 151-742, Korea

E-mail: wchoe@mail.kaist.ac.kr

Received 23 January 2001, in final form 19 March 2001
Published 14 June 2001
Online at stacks.iop.org/PSST/10/417

Abstract
Helicon plasmas were produced using a very high radio frequency (RF) (98 MHz) source which is commonly used for radio communication. As in the plasmas generated at lower frequency such as 13.56 MHz, E–H–W mode transitions were observed. In the helicon mode, a bright column was produced at the central part of the cylindrical plasma. Experiments using Nagoya type III antennae with different leg lengths showed that the antenna having the shortest legs produced the highest density, which suggests the importance of the antenna ring section. A study of the operation window of the helicon plasma at 98 MHz demonstrated that the H–W mode transition occurs at lower magnetic field at higher gas pressure with the RF power fixed. It was also observed that the transition arises at lower magnetic field at higher RF power with the gas pressure fixed, indicating the correlation between the three important operating parameters on helicon plasma generation and sustainment.

1. Introduction

Electron density in a typical helicon plasma ranges from about 10^{12} to 10^{13} cm^{-3} which is higher than other types of plasmas such as electron cyclotron resonance plasma, or capacitively or inductively coupled plasma even at a relatively low radio frequency (RF) input power [1–3]. This is one of the reasons why the helicon plasma has been actively under study not only for understanding the underlying physics but also for employing the plasma in industrial applications such as plasma processing for micro-electronic circuits [4, 5]. High-density low-pressure plasma sources have many application areas such as high aspect ratio dry etching with an input power density from 50 to 100 mW cm^{-3} and a wide operating pressure range from 0.1 to 10 mTorr [6].

RF plasmas have generally been produced at a frequency lower than or near 13.56 MHz. However, in recent years, advantages of high-frequency plasma processing compared with the conventional 13.56 MHz are well demonstrated by several experimental and modelling works in spite of the difficulties associated with RF impedance matching. These works report improvements in deposition rate and uniformity, etc [7–12]. For instance, very high-frequency operation at around 100 MHz enables the achievement of ion bombardment control without using dual RF sources [7, 10].

An RF source of around 13.56 MHz has also widely been used for generating helicon plasmas, which is in between the lower hybrid and electron cyclotron frequencies. However, a few experiments were carried out at frequencies other than 13.56 MHz, for instance at about 7 MHz, to explain the heating mechanism in helicon plasmas. Some of the results carried out below 30 MHz indicate that helicon plasma generation at frequencies much higher than 13.56 MHz is not very effective [13, 14]. However, there are no reports to date about the efficiency of helicon plasma production at very high radio frequency (VHF).

The work presented in this article started as part of the work to develop a compact ion source for proton accelerators [15] using a high-density helicon plasma. Since a low-inductance antenna matches well with a higher RF source as far as impedance matching is concerned, a VHF RF source

[3] Permanent address: Semiconductor Research and Development Center, Samsung Electronics Co, Kyungki-do 449-900, Korea.
[4] Author to whom correspondence should be addressed.

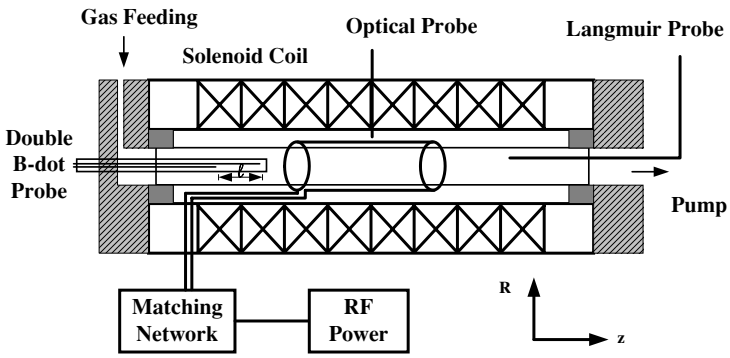

Figure 1. Schematic diagram of the helicon plasma source used for experiments. A Nagoya type III antenna is shown.

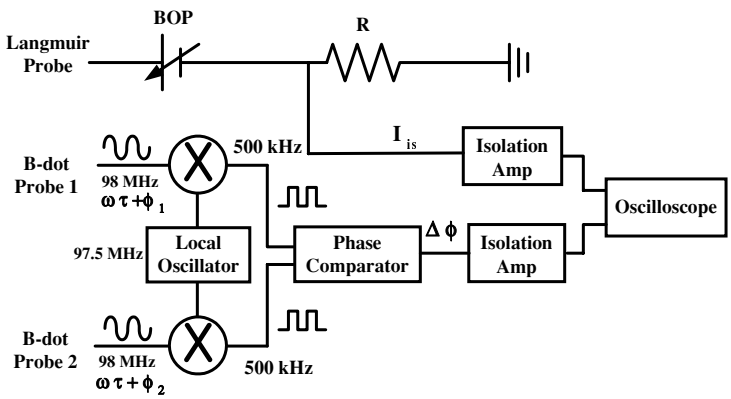

Figure 2. Schematic diagram of phase difference and Langmuir probe measurements.

may be applicable in developing a compact helicon plasma with a small sized antenna. Based on this motivation, a helicon plasma study was performed at VHF (98 MHz), which is commonly used in radio communication.

2. Description of experimental set-up

A schematic diagram of the helicon plasma source used for the experiment is shown in figure 1. The pyrex discharge tube is 2 inch in diameter and 30 cm in length, and is connected to a multi-port diagnostic chamber. A turbo-molecular pump and a mechanical pump are connected to the diagnostic chamber for providing the base pressure as low as 10^{-7} Torr. The axial magnetic field required for helicon plasma generation is provided by eight electromagnetic coils. They generate a uniform solenoidal magnetic field from $z = -9$ to +9 cm, where $z = 0$ corresponds to the axial centre of the discharge tube. The maximum field obtained is 800 G with less than 2% field ripple measured by a Gauss-meter at various positions. For field uniformity, the inner six and the outer two coils are connected separately in series, and two separate dc power supplies are used to supply different currents. The frequency of the RF generator is 98 MHz with a variable power up to 100 W. Since impedance matching between the RF generator and the helicon antenna at this high frequency is non-trivial, double loop ($m = 0$) and Nagoya type III ($m = \pm 1$) antennae utilized for experiments were made of silver-coated copper for lower antenna resistance. The resistance and inductance of the Nagoya type III antenna of 3 cm length and 5.5 cm diameter were 0.1 Ω and 430 nH, respectively, at 98 MHz.

Plasma diagnostics were performed mainly by Langmuir probes and a double B-dot probe that was installed either upstream or downstream. It is assumed that the wave motion inside a cylindrical plasma is described as $\exp[\mathrm{i}(m\theta + k_\parallel z - \omega t)]$, where θ, z are azimuthal and axial coordinates, respectively, and m and $k_\parallel$ are azimuthal mode number and axial wavenumber, respectively. Then, a double B-dot probe aligned along the z-axis produces a phase difference at a given plasma position. If one probe (reference) in a double B-dot probe is located at a specific position and the other (probing probe) is separated by a distance, ℓ, the axial wavenumber can be simply obtained by the measured phase difference $\Delta\phi$ from the relation $k_\parallel = \Delta\phi/\ell$. Measurements were done with the reference probe fixed while axially moving the probing probe with ℓ being shorter than the measured wavelength. Each probe has two windings of 2 mm in diameter. The number of turns of each probe was chosen to minimize the unwanted RF pick-up and at the same time to maximize the output signal for ease of phase comparison. Detailed descriptions on the heterodyne phase detection and the accuracy of the phase measurements are given in [16].

The plasma density and temperature deduced from the ion saturation current and the I–V characteristic curve were measured by a RF-compensated Langmuir probe [17, 18], simultaneously with the double B-dot probe (figure 2). The diameter of the Langmuir probe tip was 1 mm and it was encased in a 1/4 inch stainless-steel tubing that provided electrostatic shielding. It was located downstream in the z-direction.

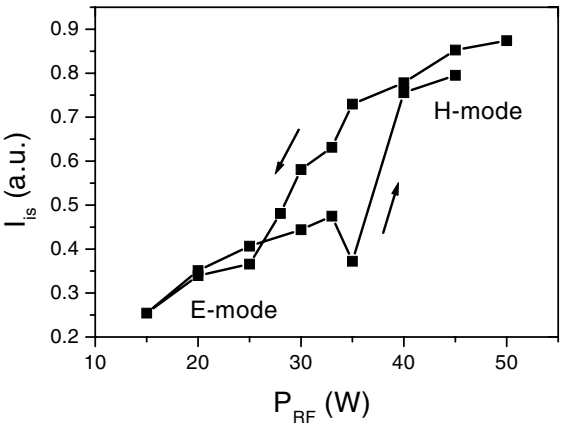

Figure 3. E–H transition characteristics shown by Langmuir probe measurement. The ion saturation current versus RF power shows hysteresis near 30 W. The experiment was performed at 1.5 mTorr argon gas pressure and no external magnetic field was applied. A Nagoya type III antenna was used.

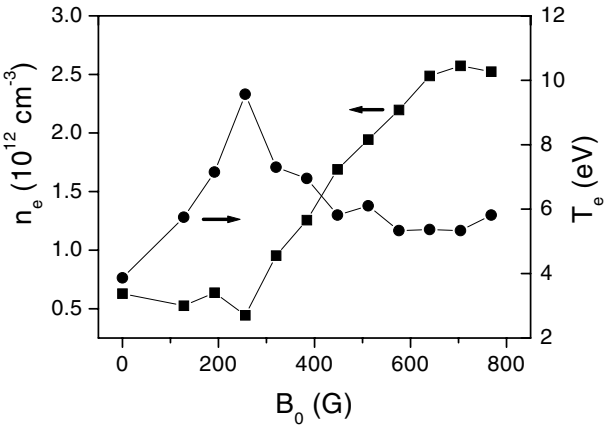

Figure 4. The electron density measured by a Langmuir probe shows a density jump near 250 G. The electron temperature increases with field strength at low magnetic field. At 250–300 G, however, it suddenly decreases indicating a dramatic change inside the plasma. Argon, 6 mTorr, 60 W, Nagoya type III antenna.

3. Results and discussion

The experiment was first performed without applying the external magnetic field to observe any mode change in the plasma produced at 98 MHz. Similar to the lower-frequency case such as 13.56 MHz, the plasma was initiated in the capacitive E-mode and subsequently it was transformed to the inductive H-mode by increasing the RF power, as shown in figure 3, where the power dependence of ion saturation current is depicted. Hysteresis is also seen. The E–H transition occurred approximately at 30 W RF power which is about 50 mW cm^{-3} considering the volume of the discharge tube. In this experiment, the gas was mainly argon at 1.5 mTorr, unless noted otherwise.

In order to study helicon wave launch and propagation, an axial magnetic field was imposed continuously from $B_0 = 0$ to 800 G by increasing the coil current with a 0.1 Hz triangular waveform. With the axial magnetic field applied, plasma confinement in the radial direction was improved and it brought about a significant increase in plasma brightness. In the presence of a sufficiently large magnetic field (>250 G) and RF power (>30 W), a bright column that generally appears in helicon plasmas was observed at the centre of the cylindrical plasma along the z-axis. The RF matching condition also changed abruptly at $B_0 \simeq 250$ G, where B_0 is the applied magnetic field.

Figure 4 shows the density and temperature measured by a Langmuir probe inserted axially at the radial centre. As shown in the figure, the density significantly increases at $B_0 >$ 250 G, being proportional to the applied magnetic field until saturation at about 700 G. This is consistent with the helicon wave dispersion relation at a fixed wavenumber. However, the electron temperature shows much different behaviour in that the initially increased temperature decreased after helicon mode (W-mode) transition at $B_0 \simeq 250$ G. The argon gas pressure in this case was 6 mTorr. Furthermore, the plasma potential measured by an emissive probe decreased from 22 to 16 V as B_0 increased. These results roughly agree with typical helicon plasmas produced by other 13.56 MHz RF sources. The obtained density is also comparable [19].

Figure 5 depicts the cross-sectional view of the plasma taken by a movie camera located at one end of the cylindrical plasma. The brightness of each frame corresponds to axially integrated light emitted from the plasma at a particular field strength. The gas pressure was 1.5 mTorr, and the plasma was initially produced in the absence of B_0 (figure 5(a)). As the applied magnetic field increases (figures 5(b)–(e) with 50, 80, 120 and <140 G, respectively), the brightly illuminating area rotates toward one of the legs of the Nagoya type III antenna until B_0 is slightly less than 140 G. Subsequently, as $B_0 >$ 140 G, the bright part around the leg disappears, and at the same time, an even brighter part appears at the centre of the cylinder (figure 5(f)). Based on other evidence such as an abrupt increase in the ion saturation current and a sudden change in the impedance matching condition, the field strength at which H–W transition occurred was around $B_0 \simeq 140$ G. As the axial field increased further, the brightness also increased but the position of the bright part was almost unchanged.

Radial measurement of the ion saturation current shown in figure 6 supports the plasma behaviour presented in the camera pictures. Just before transition ($B_0 = 130$ G), the high-density part is located around an antenna leg. After transition ($B_0 = 250$ G), however, it is located at the centre. The ion saturation current level is higher after transition, indicating a density increase due to the helicon wave launch. Further, at higher field ($B_0 = 700$ G), there exists a large density peak at the centre indicating a central column beam, which is often seen in other helicon experiments [20]. Although it is smaller than the central column, density bumps are also observed around the antenna legs A and B as shown in the 8 mTorr, 700 G case. A similar observation was made previously by Blackwell and Chen [20], who discuss that capacitive coupling between an antenna and plasma continues in the helicon mode. This considerably contributes to plasma heating around the antenna. The plasma movement toward an antenna leg before H–W mode transition has not been clearly understood, and a more thorough study will be made.

As shown in figure 1, a Nagoya type III antenna consists of a ring on each end and two legs which connect the rings. In order to find out the effect from the legs, experiments were

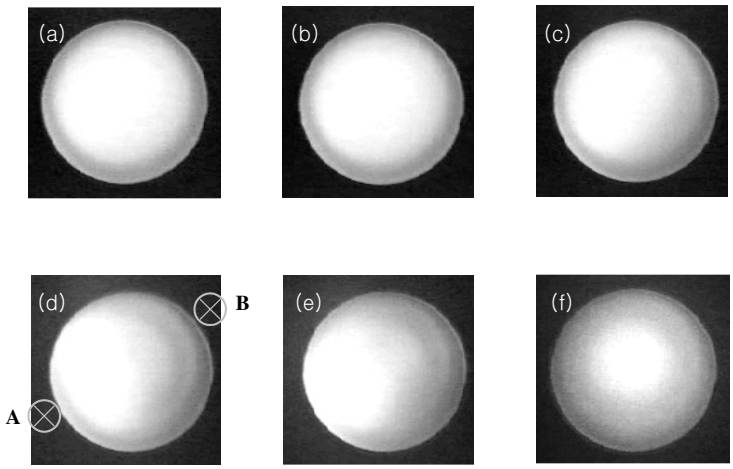

Figure 5. Pictures showing the plasma cross section with magnetic field variation. (a) 0 G, (b) 50 G, (c) 80 G, (d) 120 G, (e) <140 G (before transition), (f) >140 G (after transition). A and B denote location of Nagoya type III antenna legs. Argon, 1.5 mTorr, 55 W.

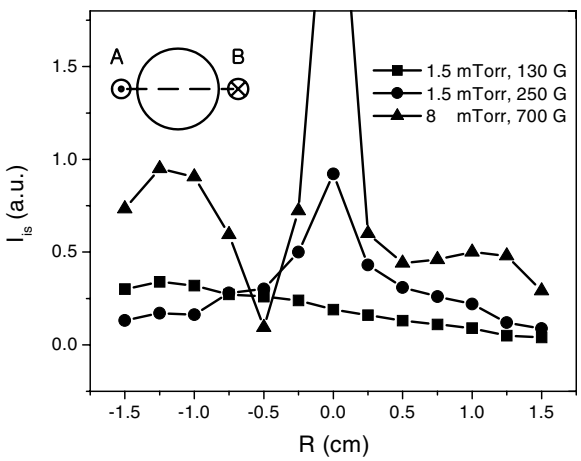

Figure 6. Radial profile of the ion saturation current. A and B denote location of Nagoya type III antenna legs. Argon, 65 W, Nagoya type III antenna.

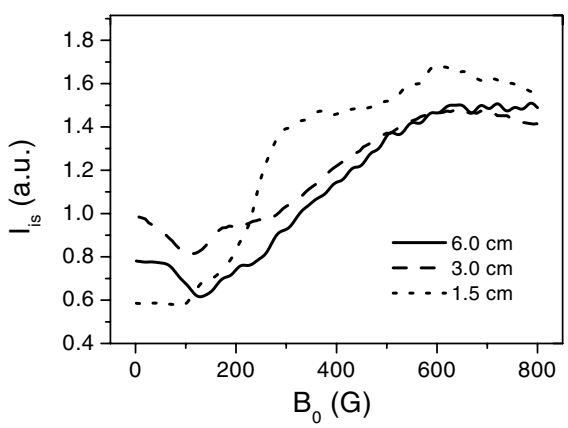

Figure 7. Ion saturation current for different antenna lengths. Argon, 65 W, 1.5 mTorr, Nagoya type III antenna.

attempted using three different antennae of lengths 1.5, 3.0 and 6.0 cm. Figure 7 depicts the measured ion saturation current versus magnetic field where the 1.5 cm antenna produces a higher density compared with the other longer antennae

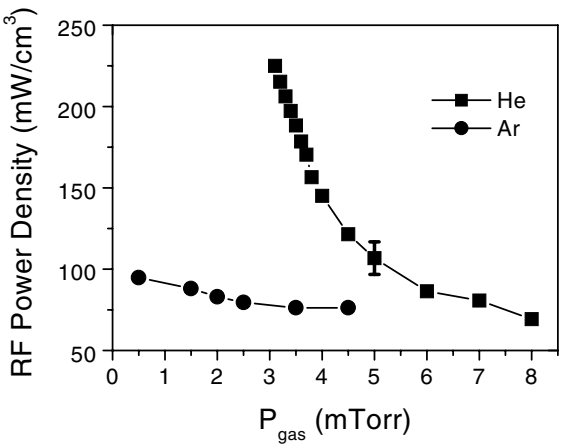

Figure 8. RF threshold power density as a function of gas pressure where H–W transition occurs. For helium, the plasma diameter was 1 inch and the applied field was 1.3 kG. A double loop antenna was used. For argon, the plasma diameter was 2 inch with 600 G applied field using a Nagoya type III antenna.

after the plasma enters helicon mode. Since the diameter of the antenna ring section was the same for all three cases and the other experimental conditions were fixed, it is thought that the density response is attributed to the antenna length. For the 1.5 cm antenna, the ratio of the ring section diameter to the leg length is higher than other antennae so that the contribution of the leg section seems to be less important. Therefore, it is suggested that the ring section plays the more important role in the helicon plasma. On the other hand, the ion saturation current is different for each antenna case at very low magnetic field. This is because each antenna having different impedance shows different capacitive and inductive effects.

To investigate the operational window of the helicon plasma driven by a 98 MHz RF source, the relation between gas pressure and threshold RF power at which the H–W mode transition occurs has been studied with two different gases, helium and argon. The axial magnetic field was large enough to ensure a mode transition that was confirmed by an abrupt change in the impedance matching condition and ion saturation current. Figure 8 shows the experimental result where RF

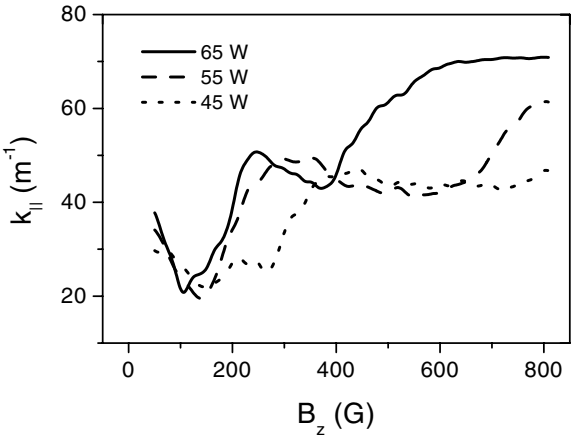

Figure 9. Wavenumber measured by a double B-dot probe at different RF power levels. The $k_{\parallel}$ jump occurs at lower magnetic field as the RF power increases. Argon, 1 mTorr, Nagoya type III antenna.

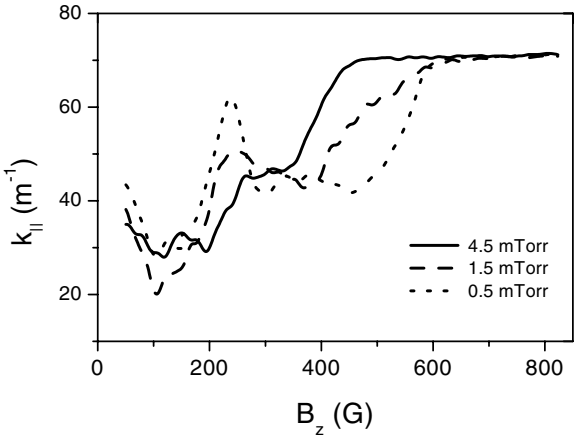

Figure 10. Wavenumber measured at different gas pressures. The $k_{\parallel}$ jump occurs at lower magnetic field as the gas pressure increases at sufficiently high magnetic field ($B_0 > 500$ G). Argon, 65 W, Nagoya type III antenna.

threshold power density versus gas pressure at fixed external field ($B_0 = 600$ G) is depicted. First, it was observed that higher pressure was required for helium than for argon. The helium plasma could not be maintained at pressures less than about 3 mTorr, whereas argon plasma could be maintained as low as 0.5 mTorr. This is due to the residence time inside the discharge chamber for helium being shorter due to its smaller mass, resulting in faster gas depletion [21]. Second, the threshold power for helium was higher than that for argon. This is due to the higher ionization potential for helium compared with argon, considering the fact that the plasma density increases abruptly as H–W mode transition occurs. Third, the threshold power decreases with increased neutral pressure, i.e. mode transition arises more easily at higher gas pressure. During the transition, it is thought that electron heating occurs by capacitive and inductive RF power coupling as well as by the helicon wave. As neutral gas pressure increases, collisions between the heated electrons and neutrals become more frequent resulting in a shorter electron mean free path ($\lambda_{en} \propto 1/n_g$ where λ_{en} and n_g are the mean free path and neutral gas density, respectively). The decrease in λ_{en} suggests reduced electron transport parallel to the magnetic field, and it gives rise to more electrons participating in the ionization of neutrals. As a result, the mode transition can occur at lower RF power at higher pressure. At very high gas pressure, however, it was observed that the mode transition became unclear, which results in an upper limit on gas pressure. In our experiment, the operating pressure window of helicon plasma ranged from sub-mTorr to about 10 mTorr with argon gas.

The main operating parameters for helicon plasma generation are RF power, applied magnetic field, and gas pressure. In order to study how these are related with each other, one of the parameters was fixed while the relation between the other two was observed. As already seen, figure 8 shows the relation between gas pressure and RF power at fixed magnetic field. Figures 9 and 10 depict the axial wavenumber $k_{\parallel}$ measured by a double B-dot probe as the RF power and the gas pressure varies, respectively. Since an abrupt change in $k_{\parallel}$ at a particular magnetic field is associated with helicon wave launch with a specific wavelength, it is indicative of a mode transition. The figures show that the plasma experiences a multi-step change in $k_{\parallel}$ including another mode transition inside the helicon mode, and the detailed interpretation of the $k_{\parallel}$ measurement will be reported elsewhere. In this article, however, the discussions are narrowed around 600 G at which figure 8 is obtained.

In figure 9 where gas pressure is fixed, mode transition occurs at lower magnetic field with larger applied RF power. This can be explained as follows. In the presence of a time-varying electric field ($E \propto \exp(i\omega t)$), the collisionless plasma conductivity perpendicular to the magnetic field is $\sigma_{\perp} \propto 1/B_0^2$ for $\omega \ll \Omega_e$ where $\Omega_e = eB_0/m_e$ [22]. The perpendicular skin depth is then $\delta_{\perp} \propto 1/\sqrt{\sigma_{\perp}} \propto B_0$. On the other hand, since the RF power density (ordinate of figure 8) is proportional to E^2, figure 8 can be considered as a part of the Paschen curve with the abscissa equal to the gas pressure multiplied by skin depth where the electric field is strong. Therefore, as the RF power increases at fixed gas pressure, $\delta_{\perp}$ decreases following the Paschen curve, as does the magnetic field for mode transition.

Finally, the gas pressure versus magnetic field was examined at constant RF power, and the result is shown in figure 10. The RF power was 65 W in this case which is large enough for ensuring mode transition with an appropriate magnetic field strength. The result shows that the mode transition occurs at lower magnetic field strength at higher gas pressure ($B_0 > 500$ G), which is in agreement with figure 8. From figures 8–10, we can see that the three important operating parameters (RF power, magnetic field, and gas pressure) are related to each other for helicon plasma generation.

4. Summary

Helicon plasmas were successfully generated at VHF (98 MHz) as part of the work to develop a high-density compact plasma source. As in the plasmas generated at lower frequency, such as 13.56 MHz, the E–H–W mode transition was observed with similar plasma density. In the helicon mode, a bright column was observed at the central part of the cylindrical

plasma. Density bumps which are smaller than the cental peak were also observed around the Nagoya type III antenna legs. These are attributed to capacitive coupling.

In order to examine the effect of the legs, experiments were performed using antennae with a fixed ring section but different leg lengths. The antenna having the shortest legs produced the highest density, suggesting the more important role of the ring section on helicon plasma.

The relation between gas pressure and threshold RF power at which H–W mode transition occurs has been studied to investigate the operation window of the helicon plasma produced at 98 MHz. It is shown that the H–W mode transition arises more easily at higher gas pressure due to the reduced electron transport resulting from more frequent electron–neutral collisions. Measurement of $k_{\parallel}$ while varying the applied field at sufficiently large RF power showed that the transition to the helicon mode occurs at a lower magnetic field in the higher gas pressure case. It is also observed that the mode transition occurs at a lower magnetic field at higher RF power when the gas pressure is constant. From the results, we have seen that the three important operating parameters (RF power, magnetic field, and gas pressure) are related to each other for helicon plasma generation.

Acknowledgments

This work was partly supported by the Korea Basic Science Institute under the Korea Superconducting Tokamak Advanced Research (KSTAR) project and the Hanbit project, and also by the BK21 project.

References

[1] Boswell R W 1984 *Plasma Phys. Control. Fusion* **26** 1147
[2] Chen F F 1991 *Plasma Phys. Control. Fusion* **33** 339
[3] Chen F F 1992 *J. Vac. Sci. Technol.* A **10** 1389
[4] Sakawa Y, Koshikawa N and Shoji T 1996 *Appl. Phys. Lett.* **69** 1695
[5] Kitagawa H, Tsunoda A, Shindo H and Horiike Y 1993 *Plasma Sources Sci. Technol.* **2** 11
[6] Shamrai K P *et al* 1997 *J. Vac. Sci. Technol.* A **15** 2864
[7] Finger F *et al* 1992 *J. Appl. Phys.* **71** 5665
[8] Finger F *et al* 1994 *Appl. Phys. Lett.* **65** 2588
[9] Schwarzenbach W, Howling A A, Fivaz M, Brunner S and Hollenstein Ch 1996 *J. Vac. Sci. Technol.* A **14** 132
[10] Surendra M and Graves D B 1991 *Appl. Phys. Lett.* **59** 2091
[11] Meier J, Flueckiger R, Keppner H and Shah A, 1994 *Appl. Phys. Lett.* **65** 860
[12] Vahedi V, Birdsall C K, Lieberman M A, DiPeso G and Rognlien T D 1993 *Phys. Fluid* B **5** 2719
[13] Kwak J G *et al* 1997 *Phys. Plasmas* **4** 1463
[14] Yun S M, Kim J H and Chang H Y 1997 *J. Vac. Sci. Technol.* A **15** 673
[15] Hwang Y S, Hong I S and Eom G S 1998 *Rev. Sci. Instrum.* **69** 1344
[16] Eom G S, Kwon G C, Bae I D, Cho G and Choe W 2001 *Rev. Sci. Instrum.* **72** 410
[17] Godyak V A, Piejak R B and Alexandrovich B M 1992 *Plasma Sources Sci. Technol.* **1** 36
[18] Sudit I D and Chen F F 1994 *Plasma Sources Sci. Technol.* **3** 162
[19] Sudit I D and Chen F F 1996 *Plasma Sources Sci. Technol.* **5** 43
[20] Blackwell D D and Chen F F 1997 *Plasma Sources Sci. Technol.* **6** 569
[21] Roth J R 1991 *Vacuum Technology* (Berlin: Springer) p 200
[22] Goldston R J and Rutherford P H 1995 *Introduction to Plasma Physics* (Bristol: Institute of Physics Publishing) p 53